ORIGINAL PAPER

Molecular geometry, vibrations and electrode potentials of 2-(4,5-dihydroxy-2-methylphenyl)-2-phenyl-2H-indene-1,3-dione; experimental and theoretical attempts

Siavash Riahi · Mohammad Reza Ganjali ·
Abdolmajid Bayandori Moghaddam · Parviz Norouzi

Abstract The electrode potential of 2-(4,5-dihydroxy-2-methylphenyl)-2-phenyl-2H-indene-1,3-dione (DMPID) in acetonitrile has been calculated. The calculations were performed using ab initio molecular orbital calculations (HF), and density functional theory (DFT) with the inclusion of entropic and thermochemical corrections to yield free energies of redox reactions. The electrode potential of DMPID was also obtained experimentally with the aid of an electrochemical technique (cyclic voltammetry). The values for geometric parameters and the vibrational frequencies of DMPID and 2-(6-methyl-3,4-dioxocyclohexa-1,5-dienyl)-2-phenyl-2H-indene-1,3-dione (MDPID) were also computed using the same levels with the basis set of 6-31G (d). The calculated IR spectrum of DMPID used for the assignment of IR frequencies was observed in the experimental FT-IR spectrum and the calculated IR and FT-IR observed spectra of DMPID were compared with correlation factor of 0.996. It should be mentioned that the present work is the first research on coagulant derivative molecules in which the electrode potential of a molecule is calculated.

Keywords Anticoagulant compound · Cyclic voltammetrey · DFT calculations · Electrode potentials · IR spectrum

S. Riahi
Institute of Petroleum Engineering, Faculty of Engineering,
University of Tehran,
Tehran, Iran

S. Riahi (✉) · M. R. Ganjali · A. B. Moghaddam · P. Norouzi
Center of Excellence in Electrochemistry, Faculty of Chemistry,
University of Tehran,
P.O. Box 14155-6455, Tehran, Iran
e-mail: riahisv@khayam.ut.ac.ir

Introduction

The search for novel anticoagulant agents has emerged as one of the most active areas of current investigation in drug discovery [1]. This is due to the large number of patients afflicted each year with thrombotic diseases [2]. Anticoagulant compounds break the vitamin K cycle by blocking the enzyme vitamin K 2,3-epoxide reductase (KO reductase) [3–5], even though other data suggest that they also inhibit another enzyme (vitamin K reductase) involved in the cycle [6–8]. Much of the recent efforts to find improved anticoagulants have been focused on the identification of compounds which, unlike warfarin, derive anticoagulant activity through direct and selective inhibition of coagulation enzymes [9]. Anticoagulant drugs fall into one of three categories: inhibitors of clotting factor synthesis, inhibitors of thrombin, and antiplatelet drugs [10]. In general, 1,3-indandione derivatives demonstrate anticoagulant properties. The synthesis and pharmacological properties of some chemicals of this category have been reported previously [11–13].

In addition, *ortho-* and *para-* dihydroxybenzenes that form a large group of compounds of natural or synthetic origin have antioxidant activities and are able to prevent auto-oxidation via inhibition of radical formation. These compounds also exhibit a wide variety of physiological and pharmacological properties [14, 15]. For these reasons, knowledge of the redox properties of these compounds is important for having a better understanding of their behavior in biological environments.

Electro-oxidation of dihydroxybenzenes is well documented. This process involves the transfer of two electrons and two protons to provide the associated quinone and the mechanism of this process was previously reported [16, 17]. In the case of the studied molecule that has anticoagulant and antioxidant properties, this process is described by Eq. (1).

$$\text{(1)}$$
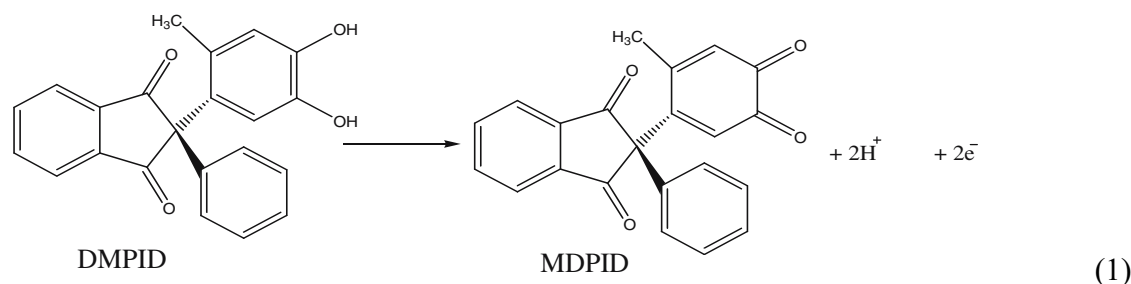
The accurate theoretical calculation of the electrode potentials plays an important role in understanding the nature of the electron-transfer reactions and the determination of molecular behaviors [18]. The ability to accurately calculate redox potentials is advantageous in different areas, particularly where the experimental measurements are difficult to achieve due to complex chemical equilibriums, and where the design of molecules with particular redox properties is of interest [19, 20]. It should be mentioned that the effects of electron-donating, electron-withdrawing and fused ring substituents on electrode potentials are important and should not be neglected. These effects have been investigated in previous papers [21–27].

In the present work, the standard electrode potential of DMPID was also calculated using the optimized structure at the same levels. The electrode potentials of DMPID were calculated in acetonitrile using PCM. Calculations have been carried out at different levels of theory. The role of frequency calculations and the relaxation part of solvation energy [28] in the improvement of the results were also investigated. The frequency studies were done on DMPID and MDPID molecules. According to our literature surveys, this is the first research concerning the studied molecule as a coagulant derivative molecule, which can also be extended to another biologically important molecules from this kind.

Calculation and experimental details

Calculations

Gas-phase molecular geometries of all species were optimized at two different levels of electronic structure theory, namely ab initio Hartree–Fock (HF) and DFT-B3LYP using 6-31G(d) basis sets. Full geometry optimizations and frequency calculations were performed and each species was found to be in a minimum by having no negative eigenvalues in the frequency calculations. The 6-31G(d) basis set includes polarization [29, 30] functions on all heavy atoms. The calculations give internal energies at 0 K. In order to obtain

gas phase free energies at 298.15 K, it is necessary to calculate the zero-point energies and thermal corrections together with entropies to convert the internal energies to Gibbs energies [22, 31]. These corrections were carried out using frequency calculations.

The next crucial step for redox potential calculations is the computation of solvation free energies. In the present study, we used the polarized continuum model (PCM) developed by Tomasi and co-workers to calculate the solvation free energies in acetonitrile [32–34]. The central idea in PCM model is the construction of a solvent-inaccessible cavity in which the solute molecule resides [34]. Gaussian 98 has been employed for all calculations [35]. The results of PCM for the calculation of electrode potentials of DMPID in acetonitrile were investigated.

The two-electron reduction potential of MDPID in acetonitrile solution was examined using 1,4-dihydroxyanthraquinone (AQH_2) as a reference compound [28–30]. Thus, MDPID can be converted to its reduced form (DMPID) according to the following isodesmic redox reaction:
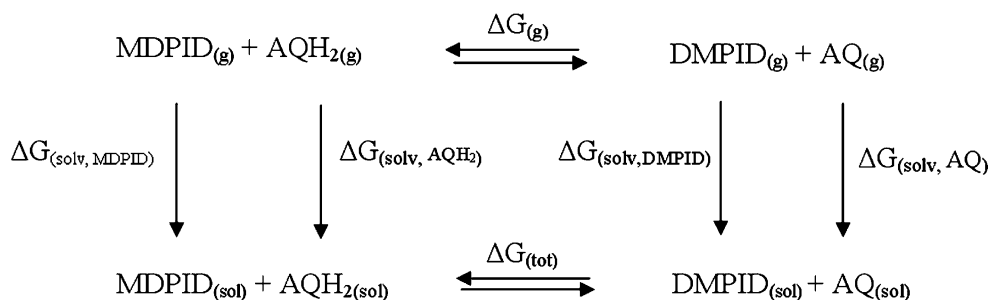
$$MDPID_{(sol)} + AQH_{2(sol)} \rightarrow DMPID_{(sol)} + AQ_{(sol)} \qquad (2)$$

Then, the formal electrode potential of MDPID, $E°'$, can be computed as:

$$\Delta G_{tot} = -2F\left(E°' - E°'_{AQ}\right) \qquad (3)$$

where ΔG_{tot} is the free energy change for reaction (2), $E°'_{AQ}$ is the experimental formal reduction potential for, 1,4-dihydroxyanthraquinone(AQ), and F is the Faraday constant. The change of Gibbs free energy for reaction (2) can be computed using the thermodynamic cycle shown in Fig. 1, which is used for the case of transferring all species involved in reaction from the gas phase into the solution phase [36]. Using this cycle, ΔG_{tot} was computed through the following expression:

$$\Delta G_{tot} = \Delta G_{gas} + \Delta G_{sol} \qquad (4)$$

$$\text{MDPID}_{(g)} + \text{AQH}_{2(g)} \quad \xrightleftharpoons{\Delta G_{(g)}} \quad \text{DMPID}_{(g)} + \text{AQ}_{(g)}$$

$$\Delta G_{(solv, MDPID)} \quad \Delta G_{(solv, AQH_2)} \quad \Delta G_{(solv, DMPID)} \quad \Delta G_{(solv, AQ)}$$

$$\text{MDPID}_{(sol)} + \text{AQH}_{2(sol)} \quad \xrightleftharpoons{\Delta G_{(tot)}} \quad \text{DMPID}_{(sol)} + \text{AQ}_{(sol)}$$

where ΔG_{gas} is the standard Gibbs energy of reaction (2) in gas phase and ΔG_{sol} is the net solvation energy in reaction (2) which is defined as follows:

$$\Delta G_{sol} = \Delta G_{AQ,sol} + \Delta G_{DMPID,sol} - \Delta G_{MDPID,sol}$$
$$- \Delta G_{AQH_2,sol} \tag{5}$$

The gas phase contribution to the Gibbs energy can be determined using ab initio calculations. Different solvation algorithms have been recently introduced for the calculation of solvation energies [37–39]. These methods are different in many ways, one of which is the modeling of the cavity created in the solvent in which the solute molecules are located. In PCM models, the solvation energy is partitioned into four components including the electrostatic interaction (ΔG_{elec}), cavity term (ΔG_{cav}), dispersion (ΔG_{dis}) and repulsion energies (ΔG_{rep}), the last three of which represent non-electrostatic interactions between the solute and the solvent.
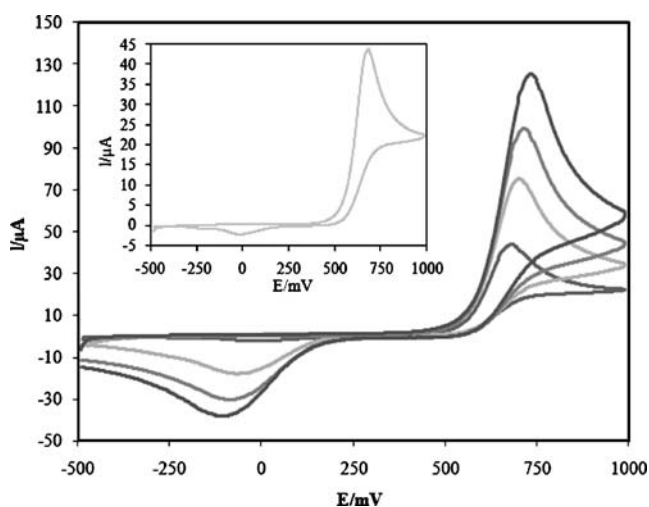
Measurments and reagents

The employed electrochemical equipment is described in the former paper [16] including a three-electrode cell; a glassy-carbon electrode as the working electrode (S = $>\pi$ mm^2), a platinum wire as the counter electrode and the homemade Ag|0.01 M AgNO$_3$ couple in the electrolyte solution as a reference electrode. All potentials are reported with respect to this reference. The cyclic voltammograms obtained in an

Fig. 2 Cyclic voltammograms of DMPID at a glassy carbon electrode (S = π mm^2) in 0.05 M LiClO$_4$-AN; Scan rates (inner to outer): 25, 80, 150 and 250 mV.s^{-1}; Inset: Cyclic voltammogram of DMPID in 25 mV.s^{-1}
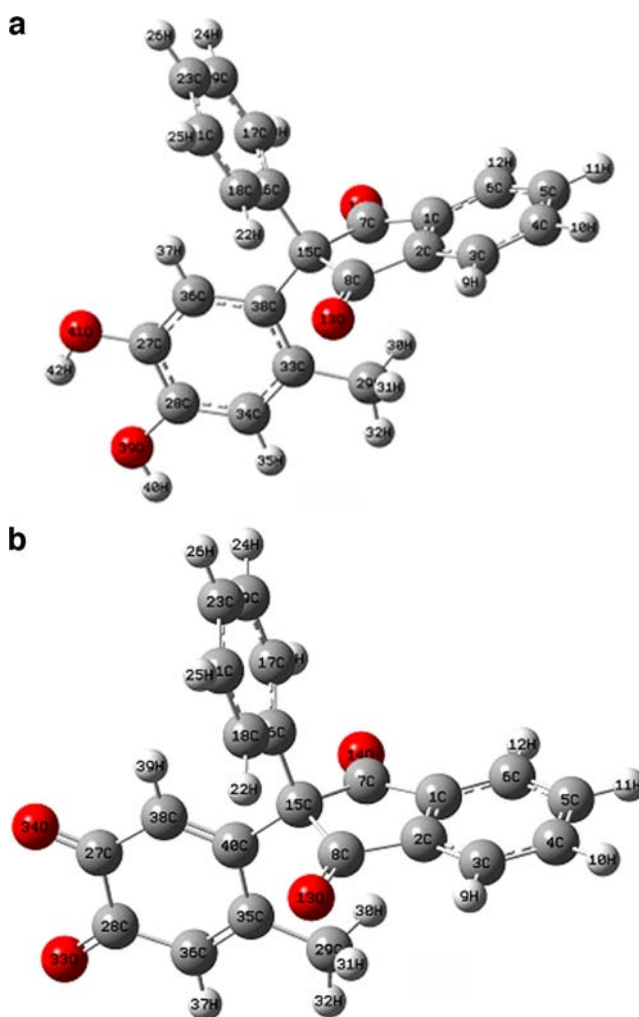

Fig. 3 Optimized structures of (**a**) DMPID and (**b**) MDPID

Table 1 The bond lengths and bond angles for both DMPID and MDPID optimized at B3LYP/6-31G(d) and HF/6-31G(d)

	DMPID			MDPID	
	B3LYP	HF		B3LYP	HF
Bond length (Å)			Bond length (Å)		
C1C7	1.488	1.488	C1C7	1.486	1.486
C2C8	1.488	1.488	C2C8	1.486	1.486
C7O14	1.215	1.189	C7O14	1.214	1.189
C7C15	1.560	1.548	C7C15	1.562	1.546
C8O13	1.215	1.189	C8O13	1.214	1.189
C8C15	1.560	1.548	C8C15	1.562	1.546
C15C16	1.552	1.552	C15C16	1.552	1.551
C15C38	1.535	1.538	C15C40	1.532	1.535
C27C28	1.399	1.382	C27C28	1.544	1.530
C27C36	1.389	1.379	C27O34	1.220	1.189
C27O41	1.365	1.351	C27C38	1.470	1.478
C28C34	1.389	1.379	C28O33	1.221	1.190
C28O39	1.377	1.360	C28C36	1.464	1.470
C29C33	1.513	1.515	C29C35	1.508	1.510
C33C34	1.401	1.390	C35C36	1.356	1.333
C33C38	1.414	1.402	C35C40	1.496	1.508
C36C38	1.401	1.391	C38C40	1.354	1.331
Bond angles(°)			Bond angles(°)		
C2C1C6	121.222	121.380	C2C1C6	121.243	121.395
C2C1C7	110.015	109.973	C2C1C7	110.065	109.935
C6C1C7	128.739	128.620	C6C1C7	128.664	128.636
C1C2C3	121.222	121.380	C1C2C3	121.243	121.396
C1C2C8	110.016	109.975	C1C2C8	110.065	109.935
C3C2C8	128.737	128.618	C3C2C8	128.663	128.635
C2C3C4	117.785	117.584	C2C3C4	117.724	117.531
C3C4C5	120.991	121.033	C3C4C5	121.031	121.070
C4C5C6	120.991	121.033	C4C5C6	121.031	121.070
C1C6C5	117.785	117.585	C1C6C5	117.724	117.531
C1C7O14	125.519	125.517	C1C7O14	126.196	126.273
C1C7C15	108.085	107.980	C1C7C15	107.798	107.699
C15C7O14	126.397	126.502	C15C7O14	126.007	126.023
C2C8O13	125.517	125.515	C2C8O13	126.195	126.272
C2C8C15	108.084	107.978	C2C8C15	107.798	107.700
C15C8O13	126.399	126.506	C15C8O13	126.007	126.023
C7C15C8	101.415	101.362	C7C15C8	101.416	101.432
C7C15C16	106.958	107.015	C7C15C16	106.967	107.140
C7C15O14	113.659	113.480	C7C15C40	113.761	113.499
C8C15C16	106.942	106.985	C8C15C16	106.948	107.136
C8C15C38	113.673	113.504	C8C15C40	113.776	113.504
C16C15C38	113.255	113.537	C16C15C40	113.049	113.228
C15C16C17	120.715	120.801	C15C16C17	120.640	120.701
C15C16C18	120.702	120.773	C15C16C18	120.619	120.704
C17C16C18	118.542	118.388	C17C16C18	118.705	118.564
C16C17C19	120.630	120.725	C16C17C19	120.528	120.624
C16C18C21	120.630	120.726	C16C18C21	120.528	120.624
C17C19C23	120.423	120.424	C17C19C23	120.404	120.391
C18C21C23	120.423	120.423	C18C21C23	120.403	120.391
C19C23C21	119.345	119.305	C19C23C21	119.426	119.397
C28C27C36	119.097	119.135	C28C27O34	120.750	120.901
C28C27O41	120.923	121.376	C28C27C38	116.930	117.000
C36C27O41	119.980	119.489	C38C27O34	122.320	122.099
C27C28C34	119.630	119.507	C27C28O33	120.704	120.726
C27C28O39	115.660	116.485	C27C28C36	116.107	116.031

Table 1 (continued)

	DMPID			MDPID	
	B3LYP	HF		B3LYP	HF
C34C28O39	124.710	124.008	C36C28O33	123.189	123.243
C29C33C34	117.754	117.395	C29C35C36	118.379	118.146
C29C33C28	123.750	124.075	C29C35C40	121.250	121.303
C34C33C38	118.497	118.530	C36C35C40	120.371	120.550
C28C34C33	121.915	122.051	C28C36C35	123.551	123.492
C27C36C38	121.917	122.119	C27C38C40	123.236	123.179
C27C36C38	121.917	122.119	C27C38C40	123.236	123.179
C15C38C33	121.505	121.778	C15C40C35	120.316	120.305
C15C36C36	119.551	119.564	C15C40C38	119.879	119.948
C33C38C36	118.944	118.658	C35C40C38	119.805	119.748
C28C39C40	109.699	111.403	Dihedral angles(°)		
C27C41C42	107.364	109.545	O34C27C38C40	179.991	−179.992
Dihedral angles(°)			O34C27C28C36	180.000	179.990
C28C27O41C42	−0.0155	−0.009	O33C28C36C35	−179.995	−179.990
C36C27O41C42	179.984	179.991	O33C28C27C38	179.993	179.993
C27C28O39C40	179.9362	179.982	C29C35C40C38	179.981	−179.989
C34C28O39C40	−0.065	−0.013	C29C35C36C28	−179.989	179.986
C29C33C34C28	−179.998	−179.995	C29C35C40C15	−0.004	0.018
C29C33C38C15	0.0096	0.012	O33C28C27O34	0.000	−0.009
C29C33C38C36	179.9952	179.986			

acetonitrile (AN) solution, contained 0.05 M of LiClO$_4$ as a supporting electrolyte.

Furthermore, the studied derivative of 1,3-dione (DMPID), was synthesized through electro-organic reactions of 4-methylcatechol and 2-phenyl-1,3-indandione [16] LiClO$_4$, AgNO$_3$ and HPLC-grade acetonitrile (Fluka) were used as received. The formal potentials (E°′) were calculated as the average of the anodic and cathodic peak potentials of the cyclic voltammogram ((E$_{pa}$ + E$_{pc}$)/2) at 25 mV.s^{-1} (Fig. 2, inset). All experiments were carried out at 25±1 °C temperature.

Results and discussion

Geometry

Optimization of the geometry is the most important step in the calculation of the standard electrode potentials. The optimized geometries and numeration of atoms in DMPID and MDPID are shown in Fig. 3. The bond lengths and bond angles for both DMPID and MDPID which were optimized at B3LYP/6-31G(d) and HF/6-31G(d) levels, are listed in Table 1. It can be seen from this table that the bond lengths and bond angles of the same molecule at B3LYP/6-31G(d) levels are in good agreement with those at HF/6-31G(d) level. Significant structural changes were caused by the oxidation of DMPID, like C-O and neighbor bond length

changes and also redistribution of atomic charges. As it is seen in Table 1 and Fig. 3a,b, the lengths of C27–O41 and C28–O39 bonds whose counterparts are C27–O34 and C28–O33 in the Ox form of DMPID, became shorter in both methods which is due to the formation of double bonding instead of single. Furthermore, the lengths of neighbor C-C bonds have also changed. The reason is that the aromatic bondings in the benzene ring have changed in to single and double bondings, i.e, C27–C28 have increased from 1.399 (B3LYP) and 1.382 Å(HF) to 1.544 and 1.530 Å, respectively. Additionlay, atomic charges of O41 and O39 have shifted toward more positive values, from −0.597 and −0.570 to −0.413 and −0.420 in the Ox form, respectively. Furthermore, atomic charges of C27 and C28 have changed from 0.303 and 0.305 to 0.374 and 0.379, respectively. C36 and C38 atomic charges values have also shifted from −0.173 and −0.161 to −0.215 and −0.187, respectively. In addition, as it is evident from Table 1, the angles around the C(15) atom are close to tetrahedral, as for a quaternary carbon. The mulliken atomic population for DMPID and MDPID were calculated using B3LYP and HF methods, i.e., carbon and oxygen mulliken atomic population using B3LYP method for DMPID structure is displayed in Fig. 4. According to DMPID atomic charges, the high negative charges are related to the oxygen atoms. The highest negative charges are located on the O39 and O41 atoms which is due to the electron donating character of the methyl group.

Fig. 4 Carbon and oxygen atomic charges for DMPID
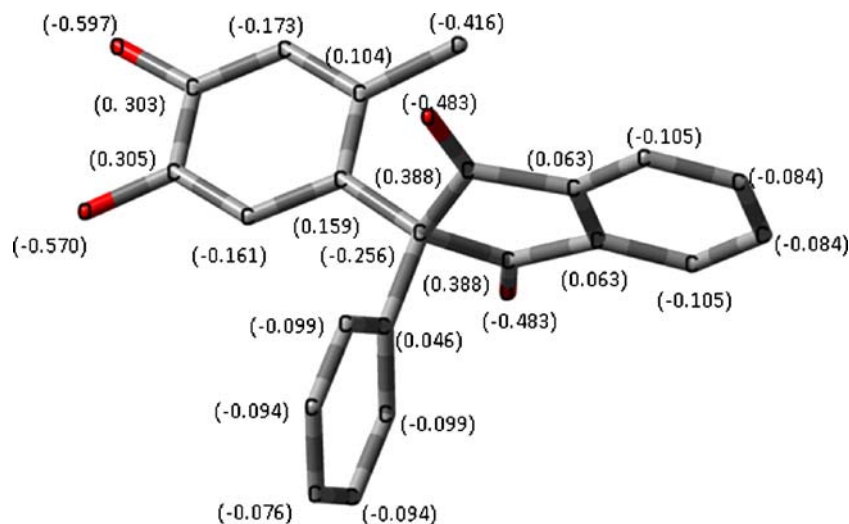
Vibration

Since MDPID, as an intermediate in an electrode process, is unstable, only an experimental spectrum of DMPID is shown in Fig. 5a. The calculations showed systematic errors between predicted and observed band positions. Scaling of the force constants according to methods reported by Schaefer and co-workers [40] and Pulay et al. [41] is a very useful way to account for systematic errors such as the neglect of anharmonic effects, basis set defects and election correlation. In many cases, the typical range for the scaling factors is from 0.8953 to 0.9986, and the scaling factors for B3LYP/6-31G(d) and HF/6-31G(d) methods were 0.8954 and 0.9614 [42]. These factors were used for predicting the vibrational spectrum of DMPID. The calculated and experimental frequencies are also summarized in Fig. 5.

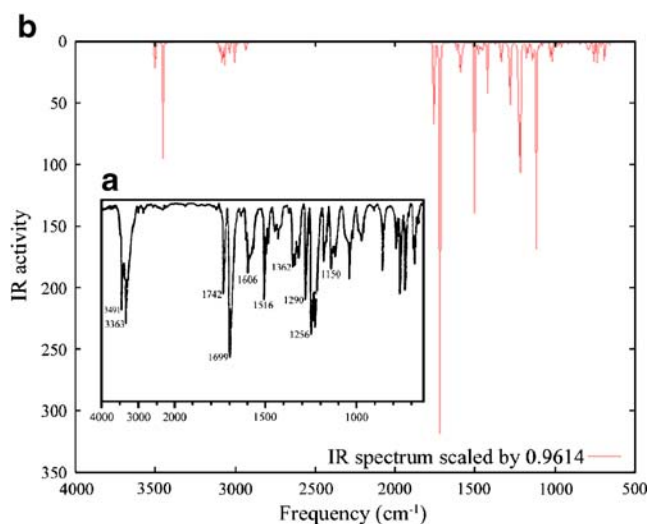Figure 5b reflects that the general appearance of the calculated spectrum is in agreement with the experimental

Fig. 5 **a**) Experimental IR spectrum of DMPID. **b**) Calculated IR spectrum of DMPID

one. The good overall agreement with experimental data for DMPID, confirms the reliability of the presented band assignment. It is concluded that the predicted spectrum for DMPID investigated here should be reliable. Because of deviations existence in the infrared intensities of the experimental data, some peaks could not be observed in the experiment, while they could be found in the calculated spectrum. It should be mentioned that only the peaks which are present in both calculated and experimental spectrum are important. Thus, we simply discussed these peaks and also some stronger peaks in the calculated spectrum.

The strongest peak in the calculated spectrum of DMPID appears at 1712 cm^{-1} (DFT method) or 1725 cm^{-1} (HF method), which represents the stretching of –C=O bond, while the strongest experimental bond is located at 1699cm^{-1}. The other band which is related to –C=O appears at 1742 cm^{-1} in the experimental spectrum, and at 1755, 1769 cm^{-1} in DFT and HF methods respectively. Two modes associated mainly with the -OH stretching of DMPID, are assigned to bands located at 3369 cm^{-1} and 3501 cm^{-1} (DFT method) or 3383 cm^{-1} and 3512 cm^{-1} (HF method) in the calculated spectrum, and their experimental frequencies appeared at 3368 and 3491 cm^{-1}. Modes calculated at 3375 cm^{-1} and 3552 cm^{-1} (DFT method) and 3398 cm^{-1} and 3763 cm^{-1} (HF method) represent the C-H stretching vibrations of aromatic and CH3 groups. Bands of -C-O- for DMPID in the calculated spectrum are located at 1357 cm^{-1}, 1294 cm^{-1}, 1256 cm^{-1} and 1145 cm^{-1} (DFT method) or 1357 cm^{-1}, 1295 cm^{-1}, 1260 cm^{-1} and 1144 cm^{-1} (HF method), while their experimental frequencies appeared at 1362 cm^{-1}, 1290 cm^{-1}, 1256 cm^{-1} and 1150 cm^{-1}, respectively. Two predicted bands of C-C stretching in DMPID ring are located at 1592 cm^{-1}, 1500 cm^{-1} (DFT method) or 1616 cm^{-1}, and 1517 cm^{-1} (HF method), and are allowed in the IR spectrum at 1606 cm^{-1}, 1516 cm^{-1}, respectively.

Table 2 The Gibbs free energy of the studied molecule for both reduced (red.) and oxidized (ox.) forms in gas phase and solution phase, along with the change of Gibbs free energy of reaction (1), ΔG_1, in both gas and solution phases

Mol.[a]	$\Delta G_{(gas)}$[b]		$\Delta G_{(sol.)}$[b]		ΔG_1(kJ mol^{-1})	
	Red.	Ox.	Red.	Ox.	Gas	Solution
1[c]	−1148.618201	−1147.392588	−1148.640320	−1147.419770	−3.418401	50.703651
2[c]	−839.064148	−837.839837	−839.103262	−837.863400	0	0
1[d]	−1141.605811	−1141.604940	−1140.433984	−1140.442113	−5.551014	53.443885
2[d]	−834.125106	−832.955394	−834.168179	−832.984996	0	0

[a] 1: Red. = AQH$_2$, Ox. = AQ, 2: Red. = DMPID, Ox. = MDPID
[b] These energies are in atomic units, Hartree (1 Hartree=2625.49975 kJ mol^{-1})
[c] These energies have been calculated at B3LYP level using 6–31G(d) basis set.
[d] These energies have been calculated at HF level using 6–31G(d) basis set.

One band is related to the in-plane C-H bending of benzene rings in MDPID, which is located at 1335 cm^{-1} (DFT method) or 1325 cm^{-1} (HF method) in the calculated spectrum and 1331 cm^{-1} in the experimental spectrum for MDPID. In conclusion the calculated IR spectrum of DMPID used for the assignment of IR frequencies was observed in the experimental FT-IR spectrum and correlations between theoretical and experimental vibrational frequencies of the DMPID molecule were 0.996.

The calculated frequencies for DMPID indicate that the optimized geometry using B3LYP/6-31G(d) method is more reliable than that optimized using HF/6-31G(d) method.

Electochemical behavior and calculation of electrode potential

Here we wish to present the calculated electrode potential of DMPID (Fig. 3a). Table 2 shows the calculated Gibbs energies of the molecules in both reduced and oxidized forms in gas phase using ab initio molecular orbital calculations (HF) and density functional theory (DFT). The basis set of 6-31G(d) was chosen considering the size of the studied molecules. Two effects are important in electrode potential calculation a) structural re-accommoda-

tion b) solvation effects [43]. Solvation energies were computed in order to convert gas-phase energies to energies in solution phase. The solute–solvent interactions, ΔG_{sol}, which are calculated using PCM models of solvation, are shown in Table 2. The solvation energies in Table 2 were obtained by optimizing the geometry of the molecules in the presence of a solvent and were also computed at the same level of theory using the basis set of 6-31G(d). This quantity was added to ΔG_{gas}, to give the change of Gibbs energy of each component in solution phase, ΔG_{sol}, according to Eq. (3).

Electrode potential of DMPID was obtained using the total Gibbs energies and the experimental value of the electrode potential of the reference molecule, AQ, in acetonitrile (Eq. (3)). Table 3 presents the electrode potentials of the studied molecule, together with the corresponding Gibbs energies of the redox reaction in acetonitrile at B3LYP/6-31 G(d) and HF/6-31 G(d) levels. From this table it can be concluded that the electrode potentials of the molecule at B3LYP/6-31G(d), and HF/6-31G(d) levels are in a good agreement with that obtained through experiments. The calculated electrode potential obtained by HF is in good agreement with the experimental value, whereas the electrode potential calculated by B3LYP method shows deviations [44]. The highest occupied molecular orbital (HOMO), the lowest unoccupied molecular orbital (LUMO), and the energy gap of HOMO and LUMO for DMPID and MDPID calculated at B3LYP/6-31G(d,p) and HF/6-31G(d) levels, are shown in Table 4. The energy of LUMO and HOMO and their energy gap

Table 3 Electrode potential of the studied molecule in acetonitrile, compared with the experimental values

Mol.[a]	Exp.($E°'$ s(V))[b]	$E°'$ (V)[c]	ΔE[d]	$E°'$ (V)[e]	ΔE[d]
1	0.599	0.599	0.000	0.599	0.000
2	0.336	0.354	0.018	0.351	0.015

[a] 1: Red. = AQH$_2$, Ox. = AQ, 2: Red. = DMPID, Ox. = MDPID
[b] Experimental values.
[c] Electrode potential calculated by Eq. (3) as explained in the text in B3LYP.
[d] Difference between experimental and theoretical.
[e] Electrode potential calculated by Eq. (3) as explained in the text in HF Differences (in V) between experimental and calculated values are shown

Table 4 Calculated amounts of HOMO and LUMO

Mol.	E_{HOMO} (eV)		E_{LUMO}(eV)		E_{LUMO}-E_{HOMO} (eV)	
	HF	B3LYP	HF	B3LYP	HF	B3LYP
DMPID	−6.85	−7.87	−0.54	−0.76	6.32	7.11
MDPID	−6.44	−6.11	−4.15	−4.95	2.29	1.15

reflect the chemical activity of the molecule. LUMO as an electron acceptor represents the ability to obtain an electron, while HOMO as an electron donor represents the ability to donate an electron. The smaller the energy gap of LUMO and HOMO, the easier it is for HOMO electrons to be excited; the higher the energies of HOMO, the easier it is for HOMO to donate electrons; the lower the energies of LUMO, the easier it is for LUMO to accept electrons. The results in Table 4 show that, the energy of LUMO in MDPID is lower than that of DMPID, and the energy gap of MDPID is smaller than that of DMPID. Therefore, the transfer of electrons from HOMO to LUMO in MDPID is relatively easier than that in DMPID, and LUMO in MDPID accepts electrons more easily with the decrease of the energies of LUMO.

Conclusions

The vibrational frequencies for DMPID and MDPID and standard electrode potential for half reaction of DMPID and MDPID were predicted using B3LYP/6-31G(d) and HF/6-31G(d) methods. The predicted standard electrode potential for half reaction of DMPID and MDPID was in agreement with the data from the experiments. (The errors may be due to considering the gases as ideal). The average discrepancy between the theory and experimental values is only 0.015 V for HF calculations; while it is 0.018 V for B3LYP. The results in this paper indicate that the HF/6-31G(d) method is superior to B3LYP/6-31G(d) method in predicting the standard electrode potentials for half reaction of DMPID and MDPID. The accuracy of PCM results with HF gas-phase calculations is the reason for the lower discrepancy. However, this theoretical method is very useful for predicting unknown standard electrode potentials of any biochemical compound. In addition, in the present work, ab initio molecular orbital calculations (HF) and density functional theory (DFT) have been employed in order to calculate charges of the atoms, Gibbs free energies and electrode potentials. Optimization of the molecules geo-mertry in the presence of a solvent, by means of PCM model of solvation at the same level of theory, was found to require a considerable amount of time for computations, especially in the case of very large molecules. Therefore, further refinements of the theory should be carried out, mainly in this regard. Consideration of bulk solvent effects is important to fully describe the experimental variations in electrode potential. Widely used PCM models reliably estimate the bulk solvent effects for the molecules.

References

1. Ripka WC, Vlasuk GP (1997) Annu Rep Med Chem 32:71–89
2. Meade WM, Miller GJ (1998) Rosenberg. Characteristics Associated with the Risk of Arterial Thrombosis. In: Verstraete M, Fuster V, Topol EJ (eds) In cardiovascular thrombosis: thrombo-cardiology and thromboneurology, 2nd edn. Lippincott-Raven, Philadelphia, pp 77–89
3. Thijssen HHW, Baars LGM (1987) J Pharmacol Exp Ther 243:1082–1088
4. Thijssen HHW, Baars LGM (1988) Br J Pharmacol 95:675–682
5. Thijssen HHW, Baars LGM (1989) Biochem Pharmacol 38:1115–1120
6. Fasco MJ, Principe LM (1982) J Biol Chem 257:4894–4901
7. Fasco MJ, Hildebrandt EF, Suttie JW (1982) J Biol Chem 257:11210–11212
8. Thijssen HHW (1995) Pestic Sci 43:73–78
9. Wiley MR, Fisher MJ (1997) Exp Opin Ther Patents 7:1265–1282
10. Pascale LR, Olwin GH (1954) Circulation 9:230–237
11. Shapiro SL, Geiger K, Freedman L (1960) J Org Chem 25:1860–1865
12. Beauregard JR, Tusing TW, Hanzal RF (1955) J Agric Food Chem 3:124–127
13. Dolmella A, Gatto S, Girardi E, Bandoli G (1999) J Mol Struct 513:177–179
14. Alanko J, Rutta A, Holm P, Mencha I, Vapaatalo H, Metsa-Ketela T (1999) Free Rad Biol Med 26:193–201
15. Yao J, Li Y, Chang M, Wu H, Yang X, Goodman JE, Liu X, Liu H, Mesecar AD, Breeman RB, Yager JD, Bolton JL (2003) Chem Res Toxicol 16:668–675
16. Bayandori Moghaddam A, Ganjali MR, Norouzi P, Latifi M (2006) Chem Pharm Bull 54:1391–1398
17. Bayandori Moghaddam A, Ganjali MR, Norouzi P, Niasari M (2007) J Electroanal Chem 601:205–210
18. Reynolds CA (1990) J Am Chem Soc 112:7545–7551
19. Reynolds CA, King PM, Richards WG (1988) Nature 334:80–82
20. Compton R, King PM, Reynolds CA, Richards WG, Waller AM (1989) J Electroanal Chem 258:79–88
21. Lister SG, Reynolds CA, Richards WG (1992) Int J Quantum Chem 41:293–310
22. Reynolds CA, King PM, Richards WG (1988) J Chem Soc Chem Commun 21:1434–1436
23. Riahi S, Bayandori Moghaddam A, Ganjali MR, Norouzi P, Niasari M (2006) J Mol Struct (Theochem) 774:107–111
24. Riahi S, Bayandori Moghaddam A, Ganjali MR, Norouzi P, Latifi M (2007) J Mol Struct (Theochem) 807:137–145
25. Riahi S, Bayandori Moghaddam A, Ganjali MR, Norouzi P (2007) J Theor Comput Chem (JTCC) 6:255–268
26. Riahi S, Bayandori Moghaddam A, Ganjali MR, Norouzi P (2007) J Theor Comput Chem (JTCC) 6:331–340
27. Riahi S, Bayandori Moghaddam A, Ganjali MR, Norouzi P (2007) J Mol Struct (Theochem) 814:131–139
28. Silva CO, Silva EC, Nascimento MAC (2000) J Phys Chem A 104:2402–2409
29. Clark T, Chandrasekhar J, Spitznagel GW, Schleyer PVR (1983) J Comput Chem 4:294–301
30. Frisch MJ, Pople JA, Binkley JS (1984) J Chem Phy 80:3265–3269
31. Winget P, Cramer CJ, Truhlar DG (2004) Theor Chem Acc 12:217–227
32. Cammi R, Tomasi J (1995) J Comput Chem 6:1449–1458
33. Cossi M, Barone V, Commi R, Tomasi J (1996) Chem Phys Lett 255:327–335
34. Tomasi J, Persico M (1994) Chem Rev 94:2027–2094
35. Frisch MJ, Trucks GW, Schlegel HB, Scuseria GE, Robb MA, Cheeseman JR, Zakrzewski VG, Montgomery JA, Stratmann RE, Burant JC, Dapprich S, Millam JM, Daniels AD, Kudin KN,

Strain MC, Farkas O, Tomasi J, Barone V, Cossi M, Cammi R, Mennucci B, Pomelli C, Adamo C, Clifford S, Ochterski J, Petersson GA, Ayala PY, Cui Q, Morokuma K, Malick DK, Rabuck AD, Raghavachari K, Foresman JB, Cioslowski J, Ortiz JV, Stefanov BB, Liu G, Liashenko A, Piskorz P, Komaromi I, Gomperts R, Martin RL, Fox DJ, Keith T, Al-Laham MA, Peng CY, Nanayakkara A, Gonzalez C, Challacombe M, Gill PMW, Johnson B, Chen W, Wong MW, Andres JL, Gonzalez C, Head-Gordon M, Replogle ES, Pople JA (1998) Gaussian Inc, Pittsburgh, PA

36. Driebergen RJ, Holthuis JJM, Blauw JS, Postma Kelder SJ, Verboom W, Reinhoud DN, Van der Linden WE (1990) Anal Chim Acta 234:285–307

37. Miertus S, Scrocco E, Tomasi J (1981) Chem Phys 55:117–129

38. Barone V, Cossi M (1998) J Phys Chem A 102:1995–2001

39. Cossi M, Barone V (2000) J Phys Chem A 104:10614–16622

40. Yamauchi Y, Frisch M, Gaw J, Schaefer HF (1986) J Chem Phys 84:2262–2278

41. Pulay D, Fogarasi G, Pang FF, Boggs JE (1979) J Am Chem Soc 101:2550–2560

42. Scott AP, Radom L (1996) J Phys Chem 100:16502–16513

43. Osorio G, Frontana C, Cuadarrama P, Frontan-uribe BA (2004) J Phys Org Chem 17:439–447

44. Namazian M, Norouzi P (2004) J Electroanal Chem 573:49–53